Fundamentals of Soil Behavior

James K. Mitchell

University of California, Berkeley

1976

John Wiley & Sons, Inc.

New York London Sydney Toronto

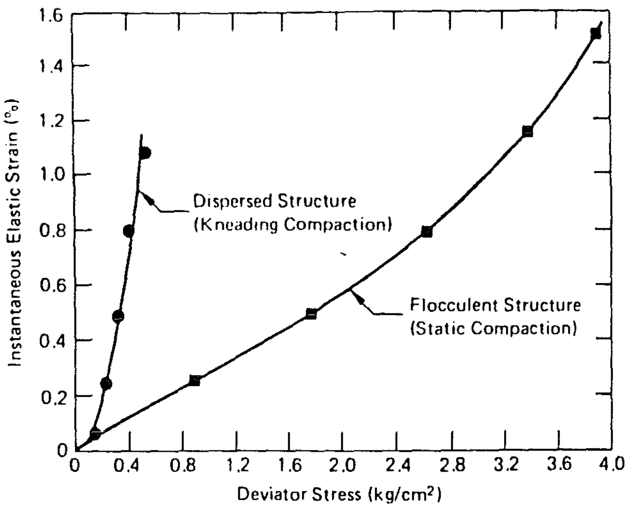

Fig. 12.25 Variations of instantaneous elastic strain with deviator stress for two different structures.

down the structure and causes a transfer of effective stress to the pore water.

Figure 12.26 is an example, and shows the results of incremental loading triaxial tests on two undisturbed and remolded samples of San Francisco bay mud. In these tests, the undisturbed sample was first brought to equilibrium under an isotropic consolidation pressure of 0.8 kg/cm^2. After undrained loading to failure, the triaxial cell was disassembled, and the sample was remolded in place. The apparatus was reassembled, and pore pressure was measured. Thus, the effective stress at the start of compression of the remolded clay was known. Stress–strain and pore pressure–strain curves for two samples, tested undisturbed and remolded, are shown in Fig. 12.26, and stress paths for Test 1 are shown in Fig. 12.27.

Differences in strength that result from fabric differences caused by differences in compaction method or from thixotropic hardening can be explained in the same way. Thus, in the absence of chemical or mineralogical changes, different strengths in two samples of the same soils at the same void ratio that result from different structures can be accounted for in terms of differences in effective stress.

Sand fabric and liquefaction

Much study of liquefaction in sands has been made in recent years because of the important role of liquefaction in soil failures during earthquakes. Liquefaction is taken here to mean* the transformation of a granular material from a solid to a liquified state as a consequence of increased pore water pressure. Cyclic loading due to earthquakes is perhaps the commonest cause of liquefaction. The resistance to liquefaction in any case depends on characteristics of the sand including gradation, particle size, and particle shape; relative density; confining pressure; and principal stress ratio (Lee and Seed, 1967*a*, 1967*b*; Seed and Lee, 1966; Seed and Peacock, 1971). It is now known (Ladd, 1974) that method of sample preparation also has a very significant effect on the resistance to liquefaction determined in the laboratory. Since differences in sample preparation have been shown to yield differences in fabric, it follows that fabric should be an important factor influencing the liquefaction potential of a sand because of the resulting differences in volume change tendencies. The importance of sample preparation method is illustrated by Fig. 12.28, which shows the relationship between cyclic stress level and number of cycles to cause liquefaction for samples of three sands prepared to the same density by two different methods.

Findings such as those shown in Fig. 12.28 suggest that more than relative density is required to characterize a given sand for liquefaction analyses. In addition, the important question arises as to how best to fabricate samples in the laboratory to duplicate the fabric in the field.

* There have been ambiguities in the use of the term liquefaction. These are discussd by Youd (1973) and are not dealt with here.

12.7 FABRIC AND PERMEABILITY

Of the properties of importance in the analysis of geotechnical problems in fine-grained soils, none is more influenced by fabric than the hydraulic conductivity or permeability. Fabric anisotropy can cause substantial permeability anisotropy. Remolding an undisturbed clay reduced the permeability of several clays by a factor of from 1 to 4, with an average of about 2 (Mitchell, 1956).

Theoretical equations for prediction of permeability (Chapter 15) based on capillary tube models for flow through porous media indicate that the flow velocity should depend on the square of the pore radius, and the flow rate on the fourth power of the radius. Thus, fabrics with a high proportion of large pore sizes are much more pervious than those with small pores. The reduction in permeability associated with remolding a soft, sensitive clay can be explained in terms of the breakdown of a flocculated open fabric and the destruction of large pores.

The profound influence of compaction water content on the permeability of a silty clay is shown in

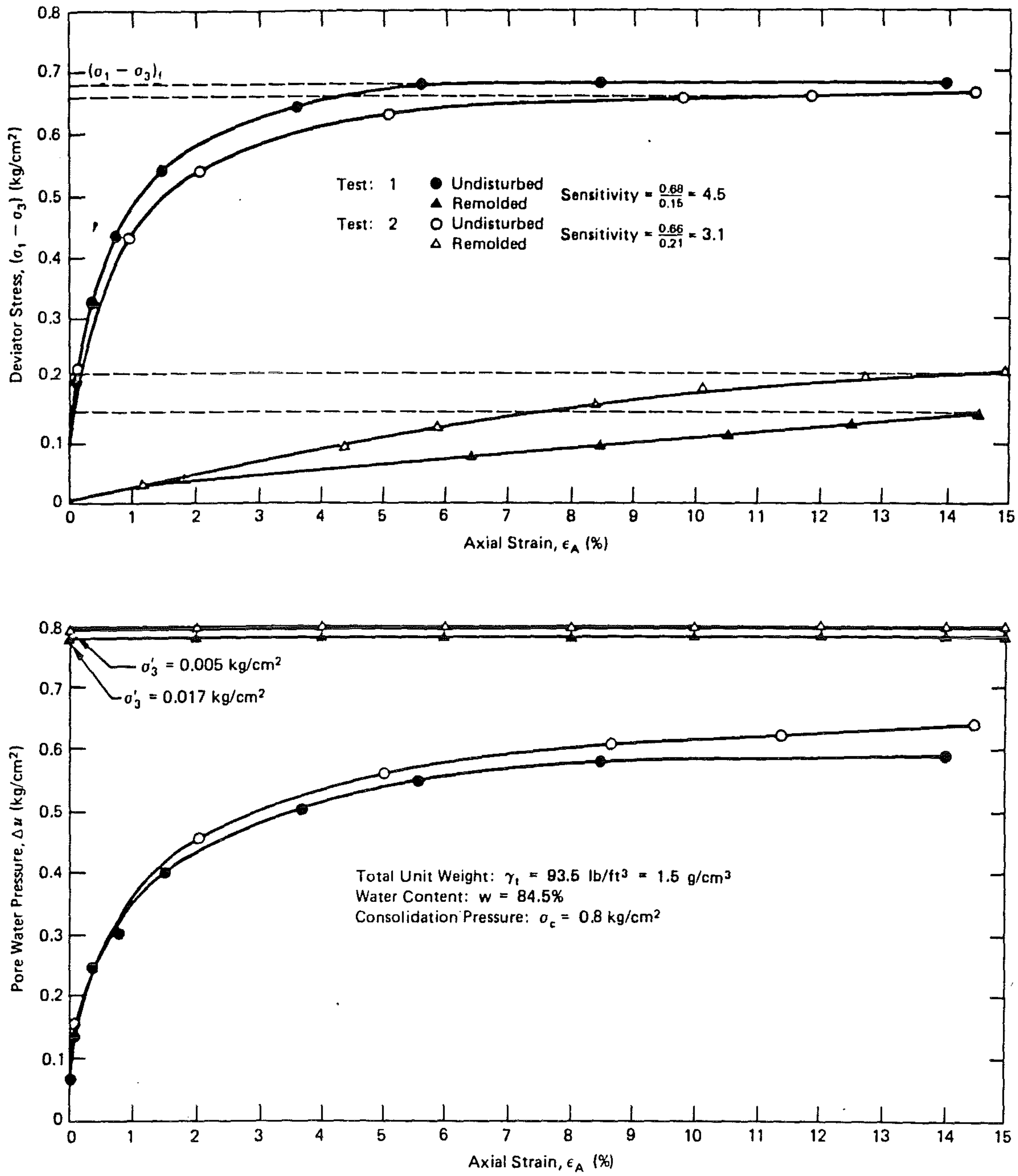

Fig. 12.26 Effect of remolding on undrained strength and pore water pressures in San Francisco Bay mud.

Fig. 12.29. This is typical of the variation of permeability with water content in compacted fine-grained soils (Mitchell, Hooper, and Campanella, 1965). For the case shown, all samples were compacted to the same density. For samples compacted using the same compactive effort, curves such as those in Fig. 12.30 are typical. For compaction dry of optimum clay particles and aggregates are flocculated, the resistance to rearrangement during compaction is high, and a fabric with comparatively large pores is formed. For higher water contents, the particle groups are weaker, and fabrics with smaller average pore sizes are formed. Considerably lower values of permeability are obtained wet of optimum in the case of kneading com-

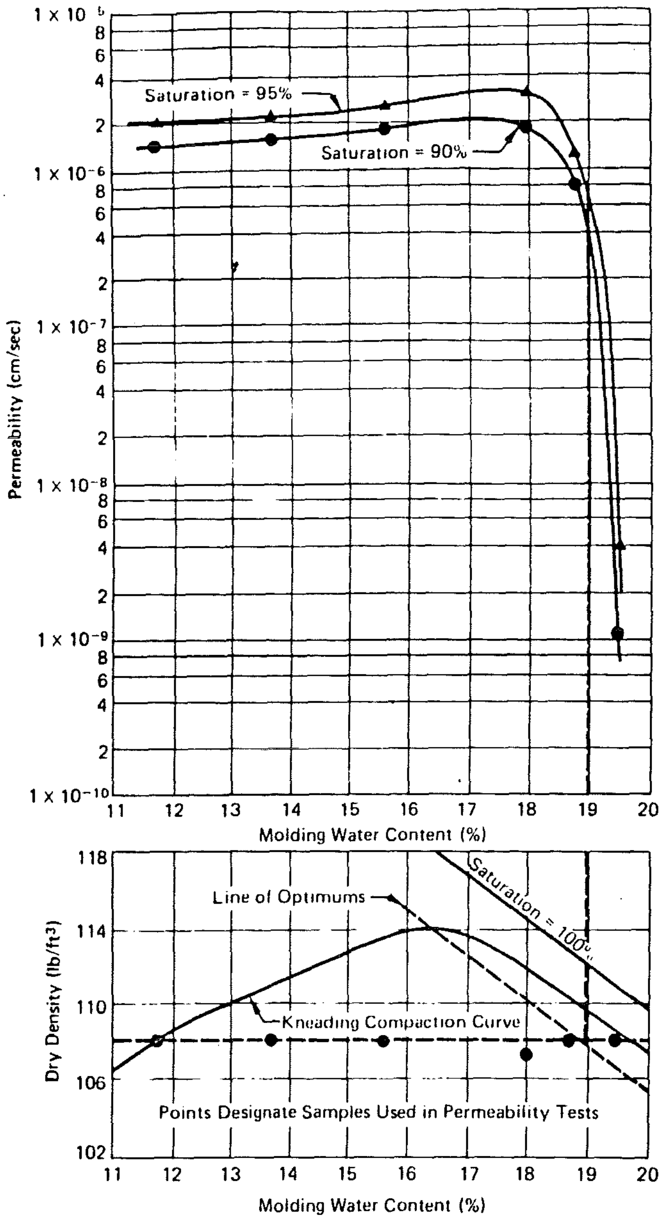

Fig. 12.29 Permeability as a function of molding water content for samples of silty clay prepared to constant density by kneading compaction.

paction than by static compaction, because the high shear strains induced in the kneading compaction method break down flocculated fabric units.

Under conditions of constant saturation and no fabric or other changes during flow Darcy's law is valid for the range of hydraulic gradients usually encountered. According to Darcy's law, the flow rate q is given by

$$q = kiA \tag{12.4}$$

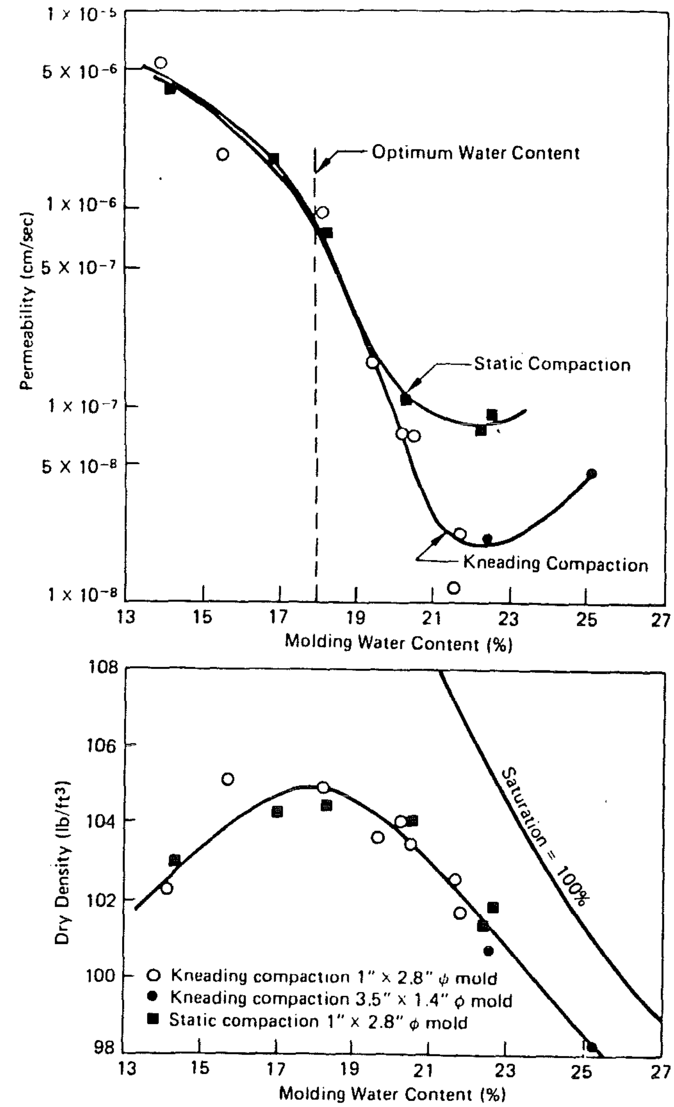

Fig. 12.30 Influence of the method of compaction on the permeability of silty clay.

where k is the hydraulic conductivity, i is the gradient, and A is the area of cross section normal to flow. The conductivity k with units of LT^{-1} is related to the "absolute permeability" K with units of L^2 by

$$K = k\left(\frac{\eta}{\gamma}\right) \tag{12.5}$$

where η and γ are the viscosity and unit weight of the pore fluid, respectively.

The well-known Kozeny–Carman equation is widely used for the prediction of K in saturated porous media:

$$K = \frac{1}{k_0 T^2 S_0^2} \frac{n^3}{(1 - n)^2} \tag{12.6}$$

In this equation, which is developed in Chapter 15, k is the pore shape factor (≈ 2.5), T is the tortuosity factor ($\sim \sqrt{2}$), S_0 is the specific surface area per unit volume of particles, and n is the porosity. Equation (12.6) is based on the assumptions that particles are approximately equidimensional, uniform, and larger than 1 μm and that flow is laminar. It has been found to work well in the case of many sands; however, it is inadequate in the case of clays (Michaels and Lin, 1954; Lambe, 1954; Olsen, 1962; and others).

The reasons for the failure of the Kozeny–Carman equation in clays provide an insight into the fabric of fine-grained soils and its relation to flocculation, dispersion, consolidation, and permeability (Olsen, 1962). The results of consolidation–permeability tests, in which the permeability is measured at a number of porosities during compression and rebound, can be compared with values predicted by equation (12.6); a typical result is shown in Fig. 12.31 for illite. Ratios of measured to predicted values as a function of porosity for several systems are shown in Fig. 12.32. Significant features of these plots are:

1. The measured permeability can be greater or less than the predicted value.
2. For compression at porosites greater than about 40 percent, the measured permeability decreases more rapidly with decreasing porosity than predicted.
3. For compression at porosities less than about 40 percent, the measured permeability decreases less rapidly than predicted.
4. For rebound, the permeability increases less rapidly than predicted.

Explanations for these discrepancies might be (Olsen, 1962):

1. Deviations from Darcy's law.
2. Electrokinetic coupling (see Chapter 15).
3. High viscosity of the pore water.
4. Tortuous flow paths.
5. Unequal pore sizes.

It may be shown that the possible effects of (1) and (2) are insignificant, and the discrepancies between predicted and measured flow rates cannot be accounted for in terms of (3) and (4).

To estimate the consequences of unequal pore sizes, the cluster model shown in Fig. 12.33 was developed (Olsen, 1962). Clusters are assumed equidimensional and of the same size. Only flow through the intercluster pores is considered, which is reasonable because of the dependence of flow rate on the fourth power of pore radius. The number of particles per cluster is N, the intracluster void ratio is e_c, and the intercluster void ratio e_p equals the total void ratio e_T less the cluster void ratio e_c.

The following relationship can be derived for the ratio of estimated flow rate for the cluster model q_{CM}, to flow rate predicted by the Kozeny–Carman equation q_{KC}:

$$\frac{q_{CM}}{q_{KC}} = N^{2/3} \frac{[1 - e_C/e_T]^3}{[1 - e_C]^{4/3}} \qquad (12.7)$$

To apply equation (12.7), an assumption must be made for the variations of e_C with e_T that occur with compression and rebound. One relationship, shown in Fig. 12.34, is based on considerations of the relative compressibilities of individual clusters and cluster as-

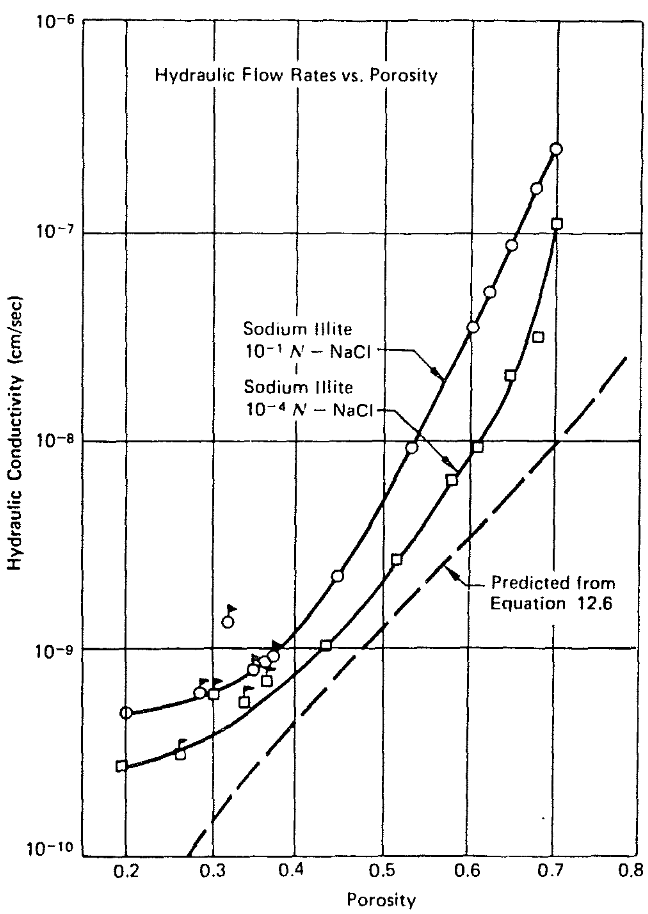

Fig. 12.31 Hydraulic flow rates as a function of porosity for illite (Olsen, 1962).

The pore shape factor k_0 has a value of about 2.5, and the tortuosity factor has a value of about $\sqrt{2}$ in porous media of approximately uniform pore sizes. Whereas the hydraulic conductivity k_h has units of velocity (LT^{-1}), the absolute permeability K has units of area (L^2).

Although the Kozeny–Carman equation works well for the description of permeability in uniformly graded sands and some silts, serious discrepancies are found in clays. Reasons for these discrepancies are discussed in some detail in Section 12.7. The major factor responsible for failure of the equation in fine-grained soils is that the fabrics of such materials do not contain uniform pore sizes (Olsen, 1962). Particles are grouped in clusters or aggregates that result in large intercluster pores and small intracluster pores.

Provided comparisons are made using samples of the same fabric, the influence of permeant on hydraulic conductivity is accounted for by the (γ_p/μ) term. If a clay is molded in different permeants, then fabrics may be quite different, and the permeability will deviate greatly from the predicted value (Michaels and Lin, 1954).

If in equation (15.25) C_s is taken to be a composite shape factor and V_s^2/S_0^2 is interpreted as a representative grain size D_s, then

$$k_h = CD_s^2\left(\frac{\gamma_w}{\mu}\right)\frac{e^3}{1+e}S^3 \tag{15.27}$$

Like the Kozeny–Carman equation, equation (15.27) describes the behavior of cohesionless soils reasonably well, but is inadequate for clays. For a uniform sand with bulky particles and a given permeant, equations (15.25) and (15.27) predict that k_h should vary directly with $e^3/(1 + e)$ and D_s^2, and experimental observations support this.

Despite the inability of equations such as (15.26) and (15.27) to predict the permeability accurately in many cases, they do reflect the overwhelming importance of pore size. Flow velocity depends on the square of pore radius, and, hence, the flow rate depends on radius to the fourth power. The specific surface term in the Kozeny–Carman equation and the representative grain size term in equation (15.27) are both measures of pore size. The hydraulic conductivity depends more on the small particles in a soil than on the large. A small percentage of fines can clog the pores of an otherwise coarse material and result in manyfold lower hydraulic conductivity.

Equation (15.27) predicts that the hydraulic conductivity should vary directly with the cube of the degree of saturation, and experimental data support this, even in the case of fine-grained soils, as may be seen in Fig. 15.5. The values shown in Fig. 15.5 were obtained under conditions of constant sample volume.

The validity of Darcy's law

As early as 1898, instances in which hydraulic flow velocity increased more than proportionally with gradient were cited (King, 1898). The absence of water flow at finite hydraulic gradients in ceramic filters of 0.1 μm average pore diameter was reported by Derjaguin and Krylov (1944), and Oakes (1960) found no detectable flow through a 30-cm long suspension of 6 percent Wyoming bentonite subjected to a 50-cm head of water. Experiments by Miller and Low (1963) led to the conclusion that there was a threshold gradient for flow in sodium montmorillonite.

Flow rates through clay-bearing sandstones were found to increase more than directly with gradient up to gradients of 170 (von Englehardt and Tunn, 1955). Deviations from Darcy's law in pure and natural clays up to gradients of 900 were measured by Lutz and Kemper (1959). Apparent deviations from Darcy's law for flow in an undisturbed soft clay are shown in Fig. 12.36 (Hansbo, 1960, 1973).

As a result of these types of observations, a number of proposals (Hansbo, 1960; Swartzendruber, 1962*a*, 1962*b*, 1963) have been made for alternative relationships to Darcy's law to describe the relationship between flow velocity and gradient. Others (Florin, 1951; Roza and Kotov, 1958; Hansbo, 1960; Barden and Berry, 1965; Mitchell and Younger, 1967; Schmidt and Westmann, 1973) have studied the implications of a threshold gradient and nonlinearity on seepage and consolidation.

Two concepts have been used to account for the nonlinearity between flow velocity and gradient: non-Newtonian water flow properties and particle migrations that cause blocking and unblocking of flow passages. The apparent existence of a threshold gradient below which flow was not detected has been attributed to a quasicrystalline water structure. It is now known that many of the effects interpreted as due to unusual water properties can be ascribed to undetected experimental errors arising from contamination of measuring systems (Olsen, 1965), local consolidation and swelling effects caused by varying effective stresses in the direction of flow, and bacterial growth

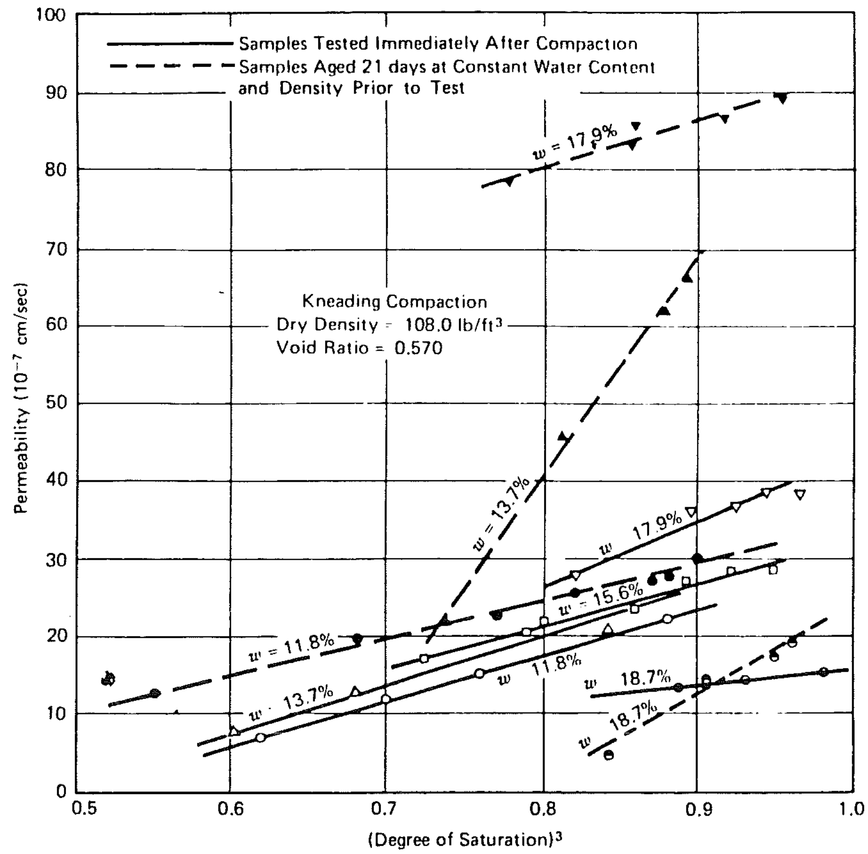

Fig. 15.5 Influence of degree of saturation on hydraulic conductivity of compacted clay.

(Gupta and Swartzendruber, 1962). Further careful measurements have failed to confirm the existence of a threshold gradient in clays (Olsen, 1965, 1969; Gray and Mitchell, 1967; Mitchell and Younger, 1967; Miller, Overman, and Peverly, 1969; Chan and Kenney, 1973). Darcy's law was obeyed exactly in the studies of Olsen (1965, 1969), Gray and Mitchell (1967), and Chan and Kenney (1973). Thus, it seems unlikely that unusual water properties can lead to non-Darcy flow behavior in clays.

On the other hand, particle migrations leading to void plugging and unplugging, electrokinetic effects, and chemical concentration gradient effects may cause apparent deviations from Darcy's law. The behavior shown in Fig. 12.36 was attributed to particle migrations under the action of seepage forces. Analysis of interparticle bond strengths in relation to the magnitudes of seepage forces leads to the conclusion that only particles not participating in the load-carrying skeleton of a soil mass are likely to be moved under moderate values of hydraulic gradient. Soils with open, flocculated fabrics and soils with a relatively low content of clay appear particularly susceptible to the movement of fine particles during permeation. Tests on saturated samples of compacted silty clay (Mitchell and Younger, 1967) indicated that particle migrations, as reflected by changes in pore pressure distribution with time in the direction of flow, were sensitive to compacted density and water content. The largest effects were found in samples compacted at the lowest water contents and densities. Variations in the fines content in a single coarse grading can influence the gradient-flow rate response significantly (Younger and Lim, 1969).

Internal swelling and dispersion of clay particles during permeation can be responsible for changes in flow rate and apparent non-Darcy behavior (Hardcastle and Mitchell, 1974). From tests on illite–silt mixtures, it was learned that the hydraulic conductivity depends on clay content, sedimentation procedure, compression rate, and electrolyte concentration. Subsequent behavior is quite sensitive to the type and

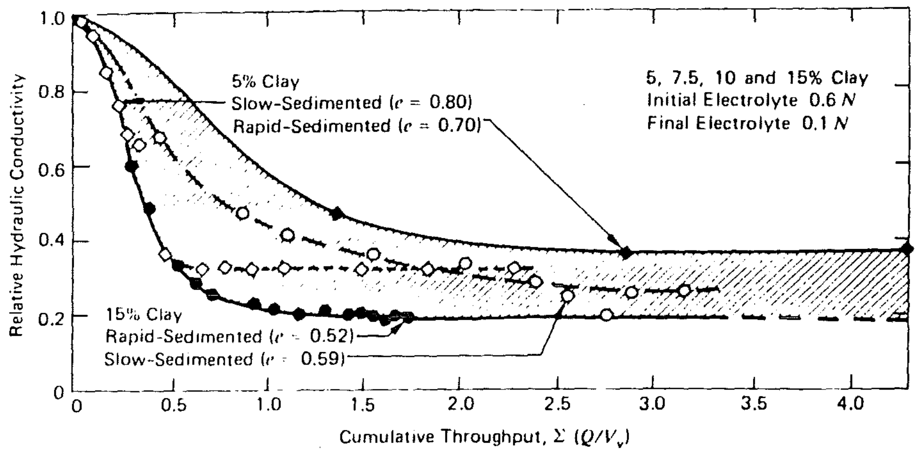

Fig. 15.6 Reduction in hydraulic conductivity as a result of internal swelling.

concentration of electrolyte used for permeation and the total throughput volume of permeant. Figure 15.6 illustrates changes in relative hydraulic conductivity that occurred while the electrolyte concentration was changed from 0.6 to 0.1 N NaCl. The cumulative throughput shown is the ratio of total flow volume at any time to sample pore volume. The hydraulic conductivities for these materials ranged from more than 1×10^{-5} to less than 1×10^{-7} cm/sec.

Practical implications. All other factors held constant, Darcy's law is valid. The only evidence to support the existence of non-Newtonian water properties or threshold gradients that cannot be accounted for by alternative explanations is that of Miller and Low (1963). On the other hand, particle migrations and fabric changes may result from seepage forces and internal swelling and dispersion brought about by changes in pore solution chemistry. Unless these effects can be shown to be of little importance, measurements should be made under conditions as closely approximating those in the field as possible.

Gradients used in laboratory determinations of hydraulic conductivity and consolidation behavior are higher than is the case for the field conditions under study. Figure 15.7 illustrates the variation of hydraulic gradient i with time factor T during consolidation according to the Terzaghi theory. The solution of the Terzaghi equation gives pore pressure as a function of position (z/H) and time factor.

$$u = \sum_{m=0}^{\infty} \frac{2u_0}{M}\left(\sin \frac{Mz}{H}\right) e^{-M^2T} \qquad (15.28)$$

where $M = \pi(2m + 1)/2$

Thus, the hydraulic gradient is

$$i = \frac{\partial}{\partial z}\left(\frac{u}{\gamma_w}\right) = \frac{2u_0}{\gamma_w H} \sum_{m=0}^{\infty} \cos\left(\frac{Mz}{H}\right) e^{-M^2T} \qquad (15.29)$$

If a parameter p is defined by

$$p = 2 \sum_{m=0}^{\infty} \cos\left(\frac{Mz}{H}\right) e^{-M^2T} \qquad (15.30)$$

equation (15.29) becomes

$$i = \frac{u_0}{\gamma_w H} p \qquad (15.31)$$

The real gradient for any layer thickness or loading intensity can be obtained by using the actual values of u_0 and H and the appropriate value of p from Fig. 15.7.

For low values of $u_0/\gamma_w H$ such as would exist in the field, for example, for $u_0 = 0.5$ kg/cm², $H = 5$ m, then $u_0/\gamma_w H = 1$, the field gradients are low throughout most of the layer thickness during the entire consolidation process. On the other hand, for a laboratory sample of 1 cm thickness and the same stress increase, $u_0/\gamma_w H$ is 500, and gradients are very large. A gradient-dependent hydraulic conductivity in such a case could be the cause of substantial discrepancies between laboratory-measured and field values of coefficient of consolidation. Constant rate of strain or constant gradient consolidation testing of such soils would be preferable to the use of load increments, as done in conventional tests, because the lower gradients would minimize particle migration effects.